ACS OMEGA

Open Access

http://pubs.acs.org/journal/acsodf

Article

Based on Spectrum-Effect Relationship, Network Pharmacology, and Molecular Docking, the Material Basis and Mechanism of Antioxidant Effect of Miao Medicine *Indigofera stachyoides* Lindl Were Studied

Gang Liu, Lingli Zhou,† Kailang Mu, Leqiang Peng, Fei Ran, Guo Feng,* and Yuchen Liu*

Cite This: *ACS Omega* 2024, 9, 42199−42211

Read Online

ACCESS | Metrics & More | Article Recommendations

ABSTRACT: *Indigofera stachyoides* Lindl (*IS*.Lindl, Xuerensen in Chinese) is a traditional medicine frequently utilized by ethnic minorities; nevertheless, the chemicals responsible for these effects have not been identified. Ultraperformance liquid chromatography (UPLC) was utilized to establish the fingerprints of various origins. Free radical scavenging in 1,1-diphenyl-2-trinitrophenylhydrazine (DPPH) and 2,2-biazobis(3-ethyl-phenylpropylthiazole-6-sulfonate) diammonium salt (ABTS) assays was used to evaluate the antioxidant activity. Partial least-squares regression analysis (PLSR) and gray correlation analysis (GRA) were utilized to determine the spectral-effect relationship in order to screen the antioxidant pharmacodynamic components. The corresponding targets were obtained from Traditional Chinese Medicine Systems Pharmacology (TCMSP) and Integrated Traditional Chinese Medicine (ITCM). Disease-related targets for antioxidants were collected from GeneCards and Online Mendelian Inheritance in Man (OMIM) databases. The PPI interaction network analysis, GO enrichment analysis, and KEGG pathway analysis were established using the online analysis platform, and Autodock software assisted in aligning the components with important targets. The fingerprint profile revealed 32 common peaks, and eight standards were identified using standard comparison, with similarity ranging from 0.920 to 0.995. The primary antioxidant components include proanthocyanidin B1, epicatechin, and proanthocyanidin B3. Important targets include EGFR, CASP3, IL6, PTGS2, and TNF. Important signaling pathways include the AGE-RAGE signaling pathways in diabetic complications, the MAPK signaling pathway, the IL-17 signaling pathway, and the pathways in cancer. The results of molecular docking technology showed that the main active ingredients of the drug could bind well to the core target. In this study, we successfully established the spectral-effect relationship of *IS*.Lindl and clarified the effective substances of *IS*.Lindl. Through network pharmacology and molecular docking methods, it was clear that *IS*.Lindl plays an antioxidant role through multicomponent, multitarget, and multipathway synergy.

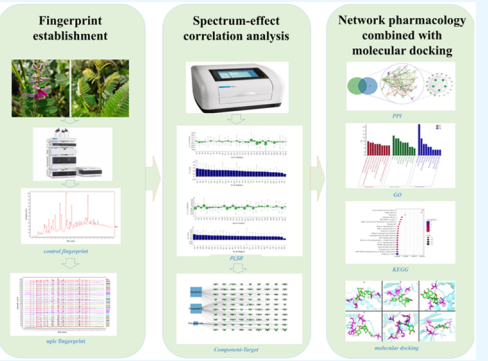

1. INTRODUCTION

Indigofera stachyoides Lindl (*IS*.Lindl, Xuerensen in Chinese) is the dried root of *Magnolia pilosa*, which is one of the traditional medicines of the Miao nationality in Guizhou, China. It possesses the efficacy of promoting blood circulation, dehumidification, and dissolving phlegm.[1] *IS*.Lindl has a variety of chemical components, with the major bioactive compounds being flavonoids, terpenes, and glycosides.[2,3] Modern pharmacological research showed that *IS*.Lindl has multiple pharmacological activities, including liver protection, antibacterial, and anti-inflammatory as well as antioxidation.[4−7] Reactive oxygen radicals are substances produced by the body during life activities. Excessive free radicals can cause damage to some cells and tissues in the body, which in turn can cause chronic diseases, aging, and cancer,[8,9] Antioxidants can scavenge free radicals and keep the organism in a healthy state, and most of the commonly used antioxidants are synthetic, toxic, and potentially carcinogenic,[10] while natural antioxidant compounds extracted from plants are safe and green.

The spectrum-effect relationship is one of the important models for studying the pharmacodynamic material basis of traditional Chinese medicine (TCM). It involves using statistical methods and fingerprint technology, along with chemometric techniques, to clarify the relationship between

Received: May 2, 2024
Revised: September 10, 2024
Accepted: September 25, 2024
Published: October 4, 2024

Table 1. Information of *IS*.Lindl Samples

NO	collection places	NO	collection places
S1	Huaxi District, Guiyang city, Guizhou, China	S14	Pan County, Liupanshui city, Guizhou, China
S2	Nanming District, Guiyang city,Guizhou, China	S15	Pan County, Liupanshui city, Guizhou, China
S3	Nanming District, Guiyang city, Guizhou, China	S16	Ceheng County, Xinyi city, Guizhou, China
S4	Nanming District, Guiyang city, Guizhou, China	S17	Changshun County, Douyun city, Guizhou, China
S5	Mallard Pond, Nanming District, Guiyang city, Guizhou, China	S18	Changshun County, Douyun city, Guizhou, China
S6	Nanming District, Guiyang city,Guizhou, China	S19	Kaiyang County, Guiyang city Guizhou, China
S7	Huaxi District, Guiyang city, Guizhou, China	S20	Kaiyang County, Guiyang city, Guizhou, China
S8	Huaxi District, Guiyang city, Guizhou, China	S21	Yangmaitian, Xiwen County, Guizhou, China
S9	Huaxi District, Guiyang city, Guizhou, China	S22	Pu'an County, Qianxinan Buyi and Miao autonomous prefecture of Guizhou Guizhou, China
S10	Wudang District, Guiyang city, Guizhou, China	S23	Xifeng County, Guiyang city, Guizhou, China
S11	Wudang District, Guiyang city, Guizhou, China	S24	Majiang, Kaili city, Guizhou, China
S12	Wudang District, Guiyang city, Guizhou, China	S25	Yunyan District, Guiyang city, Guizhou, China
S13	Pu'an County, Qianxinan Buyi and Miao autonomous prefecture of Guizhou, Guizhou, China		

the main components and their pharmacological effects. This approach allows researchers to screen out chemical components that have a strong correlation with efficacy, thereby further clarifying the pharmacodynamic material basis of TCM.[11] Network pharmacology is a multilevel network constructed by constructing a drug−disease−target and pathway. Because of its holistic and systematic characteristics, it is basically consistent with the holistic view of traditional Chinese medicine (TCM) and is widely used in the research of traditional Chinese medicine (TCM).[12,13]

At present, the literature shows that the fingerprint is used to indicate the main chemical composition and antioxidant activity of *IS*.Lindl. However, the antioxidant substances of *IS*.Lindl are not yet clear. Therefore, it is necessary to correlate the fingerprint of *IS*.Lindl with the antioxidant efficacy index to find the chemical components of the antioxidant effect of *IS*.Lindl.

In this paper, ultrahigh-performance liquid chromatography (UPLC) was used to establish the fingerprint of *IS*.Lindl of the Miao medicine. The common characteristic peaks in the fingerprint of *IS*.Lindl of the Miao medicine were identified by a reference substance comparison method. The half maximal inhibitory concentration (IC_{50}) of DPPH and ABTS free radical scavenging rates were used as pharmacodynamic indexes, and the spectrum-effect relationship model was established by combining GRA and PLSR. The correlation between characteristic peaks and antioxidant activity was further studied, and the material basis of the antioxidant activity of *IS*.Lindl was preliminarily revealed. At the same time, the antioxidant active components of *IS*.Lindl of the Miao medicine were verified by means of network pharmacology and molecular docking research methods, and the targets and pathways were clarified. This study provides theoretical support for screening the effective substances, mechanism of action, and quality evaluation of the antioxidant effect of *IS*.Lindl.

2. INSTRUMENTATION AND MATERIALS

2.1. Instrumentation. An LC-2040C 3D Plus ultrahigh-performance liquid chromatograph (PDA detector, Shimadzu, Japan), a Poroshell 120 Aq-C18 chromatographic column (2.1 mm × 150 mm, 2.7 μm), an SB-4200DTD ultrasonic cleaning machine (Ningbo Xinyi Ultrasonic Equipment Co., Ltd.), an SHZ-DIII circulating water multipurpose vacuum pump (Shanghai Iyoin Instrument Co., Ltd.), a Skanlt Software 6.1.1 full-wavelength enzyme labeler (Thermo Fisher Scientific), a FA2204B 1/10 000 balance (Shanghai Tianmei Balance Instrument Co., Ltd.), and an RHP-750A multifunctional pulverizer (Zhejiang Ronghao Industry and Trade Co., Ltd.) were used in the experiments.

2.2. Drugs and Reagents. Associate Professor Liu Gang of Guizhou University of Traditional Chinese Medicine, Guiyang, China, identified 25 batches of dried *IS*.Lindl roots that were obtained from various locations in Guizhou, China (Table 1). The suppliers of phosphoric acid, methanol, and acetonitrile (HPLC grade) were Jinshan Chemical Reagents Company in Chengdu, China, and Anhui Tiandi High Purity Solvent Company in Anhui, China. Proanthocyanidins B3 (DZP10495), Catechin (DZP10505), Proanthocyanidin B4 (DZP10903), and Epicocatechin (DZP10496) reference standards with purity ≥98% were acquired from Wanxiang Hengyuan Technology Company (Tianjin, China); Cinnamon Tannin B1 (CYK-Z0382) and Proanthocyanidin B1 (CYK-Z0382) ≥98% were acquired from Cao Yuan Kang Biological Technology Company (Chengdu, China); DPPH (20230725), ABTS (20230725), Vitc (20230817), and $K_2S_2O_8$ (20230212) were used in the experiment.

3. METHODS

3.1. Sample Solution Preparation. Twenty-five batches of *IS*.Lindl were pulverized, passed through No. 4 sieve, and weighed 0.5 g in a conical flask. This was followed by adding 60% methanol 10 mL, weighing, and sonicating for 30 min. The mixture was removed, cooled, and weighed, the weight loss was made up with 60% methanol, and the mixture was shaken. Then, the supernatant was passed through a 0.22 μm microporous filter membrane.

3.2. Standard Solution Preparation. The following ingredients: proanthocyanidin B1, proanthocyanidin B2, proanthocyanidin B3, proanthocyanidin B4, epicatechin, proanthocyanidin B1, and catechin were weighed and added to eight 5 mL volumetric flasks. The mixture of the standard solution was then diluted and dissolved with 60% methanol, shaken, and filtered through a 0.22 μm filter.

3.3. UPLC Chromatographic Conditions. The column (Infinity Lab Poroshell 120 Aq-C18, 2.1 mm × 150 mm, and 2.7 μm) was utilized with 0.1% phosphoric acid water (A):acetonitrile (B) as the mobile phase for gradient elution: 0−10 min, 9.5−12% (B); 10−40 min, 12−25% (B); 40−41 min, 25−100% (B); 41−42 min,100−100% (B); detection

https://doi.org/10.1021/acsomega.4c04212
ACS Omega 2024, 9, 42199−42211

wavelength 202 nm; volume flow rate 0.2 mL/min; column temperature 30 °C; and the volume of sample injection 3 μL.

3.4. UPLC Analysis. *3.4.1. UPLC Fingerprint Analysis Method Validation.* The precision was determined by six successive injections of one sample solution. The repeatability was carried out using six different sample solutions. The stability of the sample was determined by analyzing one sample at 0, 2, 4, 8, 12, and 24 h.

3.4.2. Fingerprint Mapping, Similarity Analysis, and Component Identification. Twenty-five batches of *IS*.Lindl herbs from different origins were taken, and the test solution was prepared according to the method under Section 3.1 and determined according to the chromatographic conditions under Section 3.3. The chromatograms were recorded and integrated manually. The chromatograms of 25 batches of samples were imported into the "Chinese Medicine Chromatographic Fingerprint Similarity Evaluation Software (2012A) Version", the solvent peaks of 0−3 min were excised, and the S1 was used as the reference chromatogram, which was corrected by multipoints and matched with the mark peaks to generate fingerprint superimposed chromatograms of 25 batches of b*IS*.Lindl and the control chromatograms (R). Also, the chromatograms of the peaks were calculated for similarity. Then, the components of the common peaks were determined by comparing the retention times with the standards.

3.4.3. Hierarchical Cluster Analysis (HCA). The peak areas of the common peaks of 25 batches of *IS*.Lindl were *Z*-sore standardized and imported into SPSS for cluster analysis. Then, HCA was performed using the scoring methods of intergroup linkage and Euclidean squared distance.

3.5. Antioxidant Activity Determination. *3.5.1. Preparation of Test Solution and Vit C Solution.* According to the preparation method of the test solution in Section 3.1, the test solution was diluted to the mass concentration of 5, 2.5, 1.25, 0.62, 0.31, 0.15, 0.07, and 0.03 mg/mL (raw drug amount). Fifty milligrams of ascorbic acid (Vit C) was weighed precisely and dissolved in 10 mL water to obtain the mother liquor of ascorbic acid standard at a concentration of 5 mg/mL. The master solution was diluted to 2.5, 1.25, 0.62, 0.31, 0.15, 0.07, and 0.03 mg/mL of the control solution.

3.5.2. DPPH Assay. The antiradical activity was determined according to the method described in the literature with a slight modification.[14] Eighty microliters of the DPPH solution (0.1 mmmol L^{-1}) was mixed with 20 μL of each sample solution at various concentrations (0.03−5 mg/mL). Ethanol 60% (20 μL) plus the sample solution (80 μL) and the DPPH solution (80 μL) were used as a blank/control.

The Vit C scavenging rate was determined according to the above method, and the reaction was carried out in the dark for 30 min. It was parallelized three times. The absorbance was determined at 517 nm by using a microplate reader. The radical scavenging activity was calculated according to the equation and the calculated IC_{50}.

$$\text{scavenging activity (\%)} = [1 - (A_{\text{sample}} - A_{\text{blank}})/A_{\text{contral}}] \times 100$$

3.5.3. ABTS Assay. The antiradical activity was determined according to the literature with a slight modification.[15] The $ABTS^{+}$ solution was prepared by mixing ABTS (7.00 mmmol L^{-1}) with an equal volume of $K_2S_2O_8$ (2.45 mmol L^{-1}) to react for 16 h in the dark. Before use, this stock solution was diluted with water to obtain an absorbance of 0.7 ± 0.02 at 734 nm. Next, 80 μL of the $ABTS^{+}$ solution was mixed with 20 μL of each sample solution at various concentrations (0.03−5 mg/mL), and ethanol 60% (20 μL) plus the sample solution (80 μL)/ABTS + solution (80 μL) was used as a blank/control.

The Vit C scavenging rate was determined according to the above method, and the reaction was carried out in the dark for 5 min, and it was parallelized three times. The absorbance was determined at 734 nm by using a microplate reader. The radical scavenging activity was calculated according to the equation and calculated IC_{50}. Scavenging activity (%) = $[1 - (A_{\text{sample}} - A_{\text{blank}})/A_{\text{contral}}] \times 100$.

3.6. Spectrum-Effect Relationship. *3.6.1. PLSR.* The relative common peaks in the fingerprints of 25 batches of samples were used as the independent variable *X*, and the antioxidant IC_{50} values were used as the dependent variable *y*. The PLSR was performed using SIMCA14.0, and the spectral regression between the common peaks and antioxidant activity was fitted to obtain the regression coefficients of each variable and the variable importance in projection (VIP).

3.6.2. GRA. Gray correlation analysis was performed between the peak area of the common peaks of the fingerprints of blood ginseng samples and the IC50 values of free radical scavenging by the antioxidant DPPH method and the ABTS method, with reference to the literature.[16] The IC_{50} value of 25 batches of *IS*.Lindl was used as the comparison sequence Xi, and 32 common peaks were used as the reference sequence X0. The original data were dimensionlessly processed by the mean method (1), and then, the absolute difference sequence (2) was calculated according to the standardized data. Before calculating the correlation coefficient, the large value and the minimum value should be calculated, followed by the maximum value (3), the minimum value (4), and then the correlation coefficient (5), ρ = 0.5. Finally, the correlation degree is calculated. The correlation degree is the average value of each correlation coefficient in the peak area reference sequence and the pharmacodynamic index comparison sequence (6).

$$.X_{\text{oi}} = \frac{X_{\text{oi}}}{\overline{X_{\text{oi}}}} \tag{1}$$

$$\Delta\text{oi}\,(k) = |X_{\text{O}}'\,(k) - X_{\text{i}}'\,(k)| \tag{2}$$

$$\Delta_{\text{i}}\,(\max) = \max \max \Delta_{\text{oi}}\,(k) \tag{3}$$

$$\Delta_{\text{i}}\,(\min) = \min \min \Delta_{\text{oi}}\,(k) \tag{4}$$

$$\delta_{\text{oi}}\,(k) = \frac{\Delta_{\text{i}}\,(\min) + \rho^{*}\Delta_{\text{i}}\,(\max)}{\Delta_{\text{oi}}\,(k) + \rho^{*}\Delta_{\text{i}}\,(\max)} \tag{5}$$

$$\gamma_{\text{oi}} = \frac{1}{n}\sum_{k=1}^{n}\delta_{\text{oi}}\,(k) \tag{6}$$

3.7. Network Pharmacology Research. *3.7.1. Component and Target Acquisition.* The key components were screened by the results of antioxidant spectroeffect relationship with positive partial least-squares regression coefficient, VIP value greater than 1, and gray correlation greater than 0.8. Then, the key components were obtained by TCMSP (http://tcmspw.com/tcmsp.php), ITCM (http://itcm.biotcm.net/), PubChem (https://pubchem.ncbi.nlm.nih.gov/) SwissTarget Prediction (http://www. swisstargetprediction) to obtain the

https://doi.org/10.1021/acsomega.4c04212
ACS Omega 2024, 9, 42199−42211

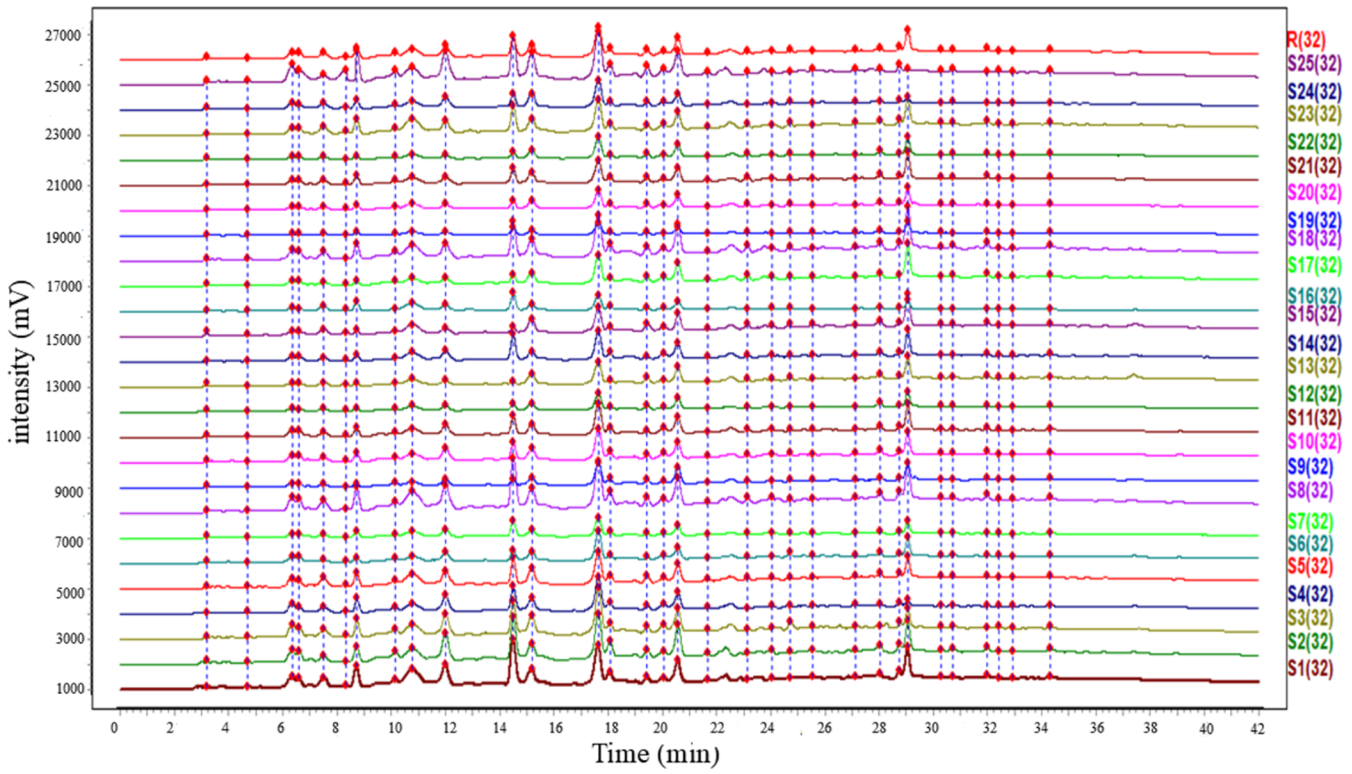

Figure 1. Fingerprint overlay of 25 batches of the *IS*.Lindl samples.

targets corresponding to the components. The target prediction and screening were performed with the threshold value of molecularly related target probability (probability) >0, and the component targets were sorted and duplicates were excluded.

3.7.2. Component-Target Network Construction. The acquired components and targets were imported into Cytoscape 3.9.1 software to construct the component-target network. The CytoNCA plug-in was applied to analyze the parameter topology of the network, and a degree was taken to rank and evaluate the component importance.

3.7.3. Acquisition of Disease Targets and Intersecting Targets. Using "Antioxidant" as the search term, we searched the GeneCards database (https://www.genecards.org/) and OMIM database (https://omim.org/) for relevant potential targets, and the disease targets from both databases were merged to remove duplicates. The constituent target genes and disease targets were imported into the Venny platform to obtain target genes common to both constituent targets and disease targets.

3.7.4. Protein−Protein Interaction (PPI) Network Analysis. To further screen target genes, the intersecting target gene names were imported into the STRING (https://www.string-db.org/) database, the protein species was set to "Homo sapiens", the minimum interaction threshold was set to 0.7, and the rest of the settings were set to the default, and the PPI network was exported in the TSV format and mapped by Cytoscape 3.9.1 software. Then, the PPI network was exported in TSV format, and the disease−drug intersection target network was drawn by the Cytoscape 3.9.1 software using the BC (Betweenness Centrality), CC (Closeness Centrality), and DC (Degree Centrality) algorithms in the cytoNCA plug-in of the software.

3.7.5. Gene Ontology (GO) Functional Enrichment Analysis and KEGG Pathway Analysis Were Performed. The component−antioxidant intersection targets were imported into the DAVID (https://david.ncifcrf.gov/) database for GO enrichment analysis and KEGG pathway analysis.

3.7.6. Molecular Docking. The active ingredients such as procyanidin A2, procyanidin B1, and epicatechin were screened by the spectral-effect relationship modeling, and the key targets IL6, PTGS2, TNF, EGRF, and CASP3 were screened by network pharmacology for molecular docking. The active ingredients were saved as the sdf by downloading the Mol2 structure from the TCMSP database as well as the 2D structure of the key ingredients from the Pubchem database, and then the mol2 file was saved by calculating the lowest energy of their MM2 using Chem3D 20.0 in ChemDraw 20.0, and the key targets were saved as mol2 by downloading the 2D structure of the key ingredients from the PDB database (http://www.rcsb.org) to download the 3D structures in the Pdb format. The target proteins were dehydrogenated and hydrogenated using the AutoDock Tools 1.5.6 software, and the active ingredients and protein targets were converted to the pdbqt format. Finally, molecular docking was performed using AutoDock Vina and visualized by Pymol software.

3.8. Data Analysis. The similarity evaluation system of the chromatographic fingerprint of traditional Chinese medicine (2012 edition) was used to analyze the fingerprint data of 25 batches of the *IS*.Lindl extract, and the similarity between *IS*.Lindl from different producing areas was calculated. The reference fingerprint (R) was automatically generated by taking the S1 sample as the control, setting the time window width to 0.1, manual correction, multipoint correction, full mark peak matching, and automatic generation of the reference fingerprint (R). IBM SPSS 26.0 software (SPSS for Windows Inc., USA) was used to cluster *IS*.Lindl from different producing

https://doi.org/10.1021/acsomega.4c04212
ACS Omega 2024, 9, 42199−42211

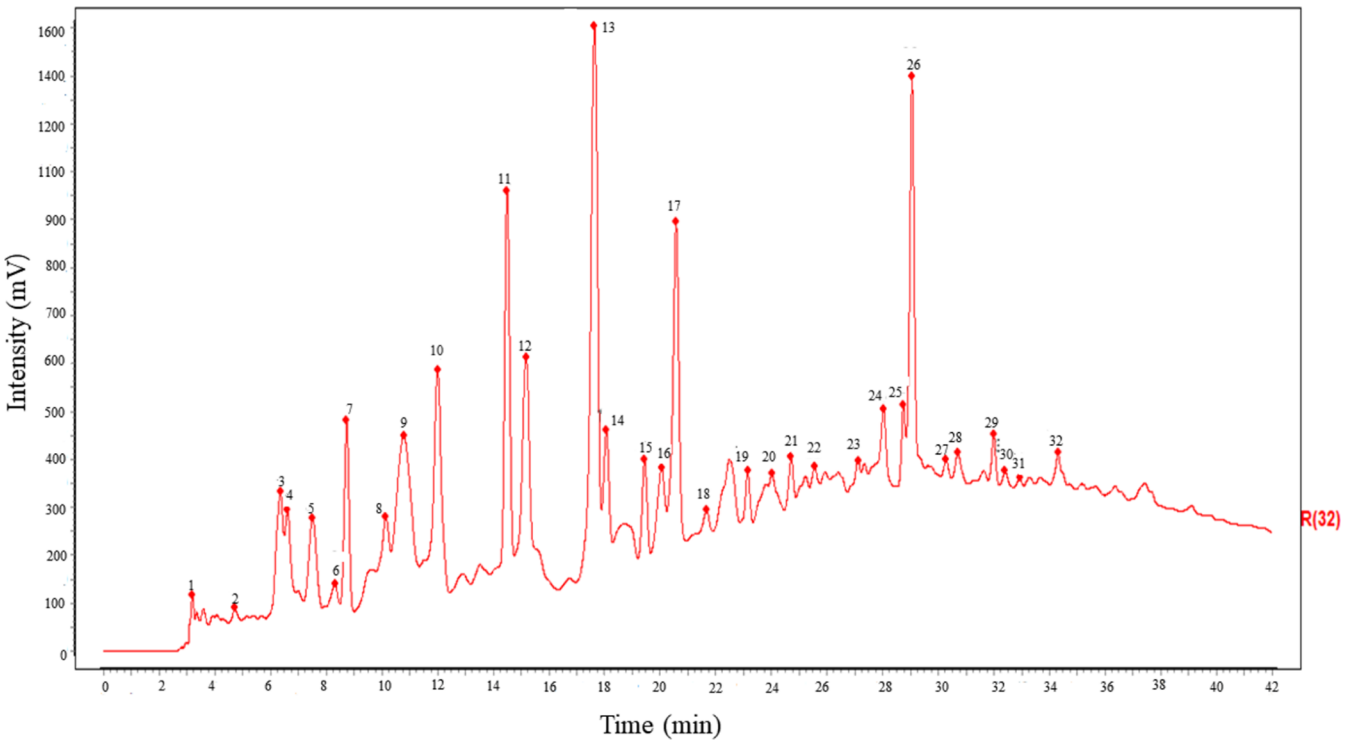

Figure 2. Reference chromatograms of the *IS*.Lindl samples: 4: proanthocyanidin B1; 5: proanthocyanidin B3; 7: catechin; 9: proanthocyanidin B4; 10: proanthocyanidin B2; 11: epicatechin; 13: cinnamtannin B-1; 26: procyanidin A2.

areas, and the intergroup connection method was used to cluster the *IS*.Lindl from different producing areas. The similarity between different samples was calculated by the square Euclidean distance. IBM SPSS and GraphPad prism 8 (GraphPad Software Inc. USA) were used to analyze the antioxidant data of *IS*.Lindl from different habitats. SIMCA14.1 (Umetrics Inc.Sweden) software was used to establish a PLSR model between the common peaks of *IS*.Lindl and antioxidant indexes. Excel 2016 (Microsoft Inc. USA) was used for GRA.

4. RESULTS AND ANALYSIS

4.1. Result of HPLC Fingerprints. *4.1.1. Method Validation.* The precision results showed that the RSD of the relative retention time of each common peak was less than 0.2%, and the RSD of the relative peak area was less than 5.0%, indicating that the precision of the instrument was good. Repeatability results showed that the RSD of the relative retention time of each common peak was less than 0.2%, and the RSD of the relative peak area was less than 5.0%, indicating that the method was reproducible. The stability results showed that the RSD of the relative retention time of the common peaks was less than 0.3%, and the RSD of the relative peak area was less than 5.0%, indicating that the stability of the test solution was good within 24 h.

4.1.2. Fingerprint Mapping, Similarity Analysis, and Component Identification. Twenty-five batches of the sample fingerprints of *IS*.Lindl were established (Figure 1), and a reference chromatogram (Figure 2) was generated with a total of 32 common peaks. The similarity of the fingerprints of 25 batches of samples was calculated, and the similarity was greater than 0.9 (Table 2). By comparing the retention times of the standard compounds, eight components were identified as peak 4 (proanthocyanidin B1), peak 5 (proanthocyanidin B3), peak 7 (catechin), peak 9 (proanthocyanidin B4), peak 10 (proanthocyanidin B2), peak 11 (epicatechin), peak 13 (cinnamon tannin B1), and peak 26 (proanthocyanidin A2).

Table 2. Similarity Evaluation Result of the *IS*.Lindl Samples

sample	similarity	sample	similarity
S1	0.969	S14	0.983
S2	0.978	S15	0.92
S3	0.987	S16	0.958
S4	0.967	S17	0.942
S5	0.992	S18	0.99
S6	0.964	S19	0.986
S7	0.994	S20	0.978
S8	0.979	S21	0.98
S9	0.953	S22	0.956
S10	0.995	S23	0.985
S11	0.992	S24	0.954
S12	0.974	S25	0.923
S13	0.922	control	1

4.1.3. HCA. Figure 3 shows that when the distance is >15, the samples can be categorized into three classes, with S10 clustered into the first class, S25, S3, S18, S2, and S1 clustered into the second class, and the rest of the batches clustered into the third class.

4.2. Oxidation Activity Aanalysis. The antioxidant capacity is expressed as a half maximal inhibitory concentration (IC_{50}), with a lower IC_{50} indicating greater antioxidant capacity. The IC_{50} of the DPPH radical was 0.0122−0.4493 mg/mL, and the IC_{50} of the ABTS radical was 0.0629−0.7525 mg/mL. The results showed that *IS*.Lindl had strong antioxidant capacity (Table 3).

https://doi.org/10.1021/acsomega.4c04212
ACS Omega 2024, 9, 42199−42211

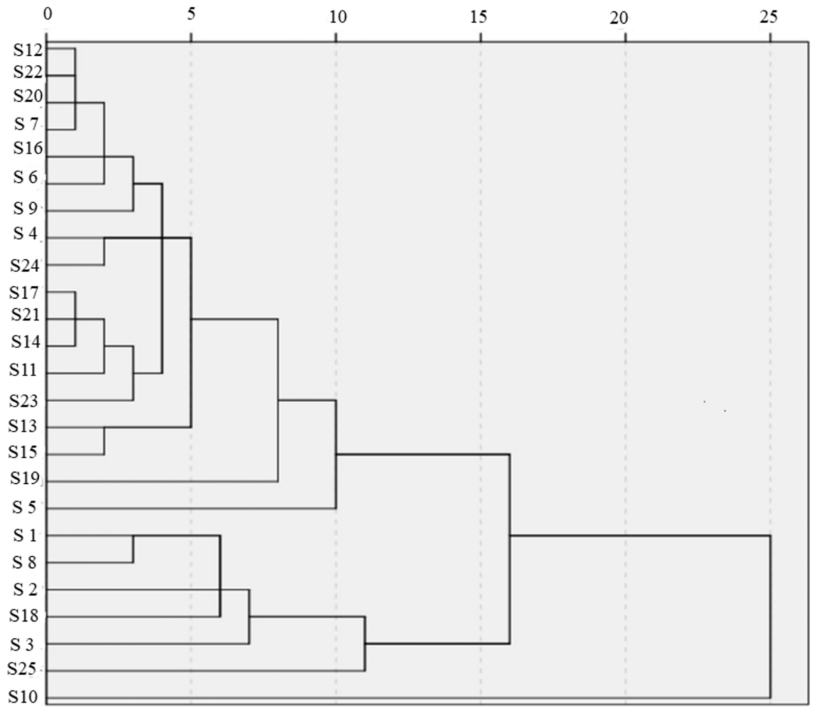

Figure 3. Hierarchical cluster analysis of 25 batches of the *IS*.Lindl samples.

Table 3. IC_{50} Values of 25 Batches of the *IS*.Lindl Samples

sample	DPPH IC_{50}(mg/mL)	$ABTS^{+}IC_{50}$(mg/mL)
S1	0.1271	0.1393
S2	0.0919	0.0913
S3	0.084	0.1988
S4	0.0906	0.1476
S5	0.1199	0.1341
S6	0.1208	0.2806
S7	0.1269	0.3689
S8	0.0555	0.1240
S9	0.1439	0.1729
S10	0.0355	0.0629
S11	0.0774	0.2183
S12	0.2373	0.5607
S13	0.0990	0.6748
S14	0.4493	0.5798
S15	0.0705	0.3853
S16	0.1053	0.6674
S17	0.0827	0.3828
S18	0.1434	0.2473
S19	0.2058	0.3195
S20	0.2452	0.7202
S21	0.3117	0.3262
S22	0.0802	0.7525
S23	0.0174	0.3822
S24	0.0409	0.3698
S25	0.0122	0.2052
Vit C	0.275	0.101

4.3. Spectral-Effect Relationship. *4.3.1. PLSR.* The greater the absolute value of the regression coefficient, the greater the contribution rate of the chemical composition represented by the chromatographic peak to the antioxidant, and the positive and negative representations of the dependent variable is positively correlated or negatively correlated with the independent variable. The variable importance in projection (VIP) is an important indicator of the explanatory power of the independent variable (ingredient) to the dependent variable (efficacy), where the larger the VIP, the greater the contribution of the ingredient to the efficacy.[17]

Figure 4 shows that the regression equation for the DPPH method is $y_{DPPH} = -0.154_{X1} + 0.073_{X2} - 0.082_{X3} + 0.143_{X4} - 0.129_{X5} - 0.067_{X6} - 0.061_{X7} - 0.031_{X8} - 0.065_{X9} - 0.030_{X10} + 0.105_{X11} - 0.162_{X12} - 0.081_{X13} + 0.115_{X14} - 0.140_{X15} - 0.075_{X16} - 0.035_{X17} - 0.152_{X18} + 0.120_{X19} + 0.047_{X20} - 0.134_{X21} - 0.0284_{X22} + 0.070_{X23} + 0.063_{X24} + 0.024_{X25} + 0.102_{X26} - 0.005_{X27} - 0.036_{X28} + 0.079_{X29} - 0.015_{X30} - 0.018_{X31} + 0.029_{X32}$, the results showed that X2, X4 (proanthocyanidin B1), X11 (epicatechin), X14, X19, X20, X23, X24, X25, X26 (proanthocyanidin A2), and X32 were positively correlated with DPPH antioxidant activity, indicating that the above chromatographic peaks may be the main components of the DPPH antioxidant activity. The VIP values of X4 (proanthocyanidin B1) and X14 and X26 (proanthocyanidin A2) were greater than 1, indicating that the antioxidant activities of these three components were significant.

Figure 5 shows that the ABTS method regression equation is $y_{ABTS} = 0.067_{X1} - 0.147_{X2} - 0.099_{X3} - 0.070_{X4} + 0.001_{X5} + 0.0104_{X6} + 0.0126_{X7} - 0.046_{X8} + 0.074_{X9} - 0.084_{X10} + 0.041_{X11} + 0.095_{X12} - 0.073_{X13} - 0.015_{X14} + 0.093_{X15} - 0.104_{X16} - 0.029_{X17} - 0.118_{X18} - 0.136_{X19} + 0.247_{X20} + 0.104_{X21} - 0.331_{X22} - 0.197_{X23} + 0.098_{X24} - 0369_{X25} + 0.105_{X26} - 0.062_{X27} - 0.219_{X28} - 0.087_{X29} - 0.059_{X30} - 0.082_{X31} - 0.027_{X32}$. The above results showed that X1, X5 (proanthocyanidin B3), X6, X7 (catechin), X9 (proanthocyanidin B4), X11 (epicatechin), X12, X15, X20, X21, X24, and X26 (proanthocyanidin A2) were positively correlated with ABTS method antioxidant activity, indicating that these chromatographic peaks may be the main components involved in ABTS reagent antioxidant activity. The VIP values of X11 (epicatechin), X20, X12, and X6 were greater than 1,

https://doi.org/10.1021/acsomega.4c04212
ACS Omega 2024, 9, 42199−42211

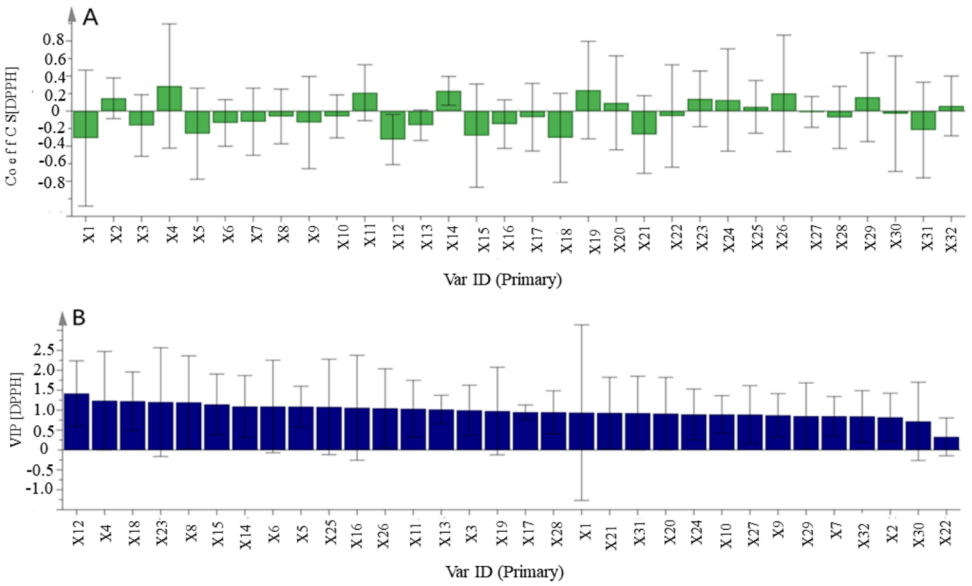

Figure 4. Regression coefficients of DPPH (A) and VIP (B) obtained with LPSR.

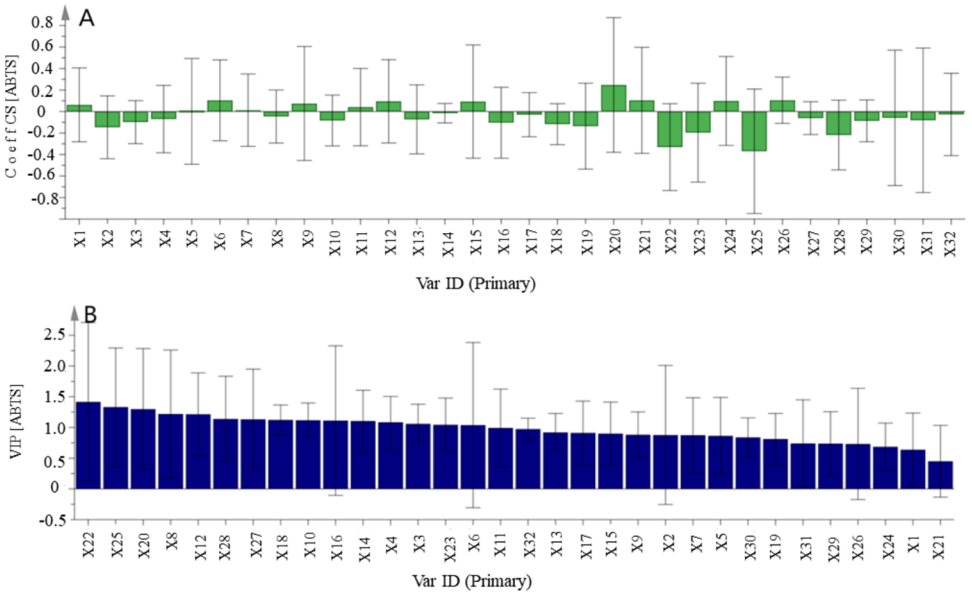

Figure 5. Regression coefficients of ABTS (A) and VIP(B) obtained with LPSR.

indicating that the three components had significant antioxidant activity against the ABTS method.

4.3.2. GRA. Generally, gray correlation greater than 6 indicates that the chromatogram peaks are correlated with that potency.[18] Table 4 shows that the correlation of 32 shared peaks with DPPH and $ABTS^{+}$ scavenging rate in 25 batches of samples were all greater than 0.75, which indicated that blood ginseng exerts its antioxidant activity as a result of the joint action of multiple components.

4.4. Cyberpharmacology Research. *4.4.1. Component Target Acquisition.* Proanthocyanidin B1, epicatechin, and proanthocyanidin A2 were conditionally screened as components for web-based pharmacological studies. Target prediction and screening were performed with probability >0 as the boundary value, and 90 related targets were obtained after sorting and deduplication.

4.4.2. Construction of Active Component-Target Network Diagram. Figure 6 is the component-target network diagram. The blue color represents the active ingredient, and the green color represents the target gene. It can be seen that each component acts on multiple targets, and the shape size in the network diagram represents the degree value, and the larger the degree value, the larger the shape.

4.4.3. Disease Targets and Intersecting Targets. The retrieved disease targets and ingredient targets were merged and deduplicated, and the Wenny diagram were plotted using the antibiotic online data analysis platform to obtain the intersecting targets of ingredients and antioxidants.

4.4.4. Protein−Protein Interaction Network Analysis. Figure 7 shows that the network includes 22 nodes and 88 edges with no isolated nodes and good connectivity, characterizing the antioxidant effects of *IS*.Lindl through the synergistic regulation of multiple components and targets. The PPI network was exported in the TSV format and the disease−drug intersection target network was drawn by Cytoscape 3.9.1 software, and the core targets IL6, PTGS2, TNF, EGFR, and

https://doi.org/10.1021/acsomega.4c04212
ACS Omega 2024, 9, 42199−42211

Table 4. Gray Correlation Analysis

peak	DPPH correlation	peak	DPPH correlation
X24	0.843	X1	0.843
X2	0.841	X24	0.838
X19	0.829	X21	0.835
X22	0.829	X31	0.834
X1	0.828	X6	0.833
X30	0.827	X13	0.826
X13	0.826	X19	0.825
X31	0.823	X17	0.823
X17	0.823	X12	0.821
X27	0.820	X15	0.821
X21	0.819	X30	0.819
X9	0.816	X2	0.818
X12	0.816	X28	0.817
X15	0.815	X26	0.813
X26	0.815	X9	0.812
X4	0.815	X29	0.810
X16	0.814	X16	0.810
X29	0.814	X5	0.809
X14	0.813	X27	0.806
X32	0.811	X4	0.805
X6	0.811	X32	0.804
X28	0.809	X20	0.804
X8	0.809	X22	0.799
X5	0.807	X14	0.790
X23	0.805	X10	0.788
X10	0.801	X3	0.786
X18	0.798	X23	0.780
X3	0.793	X11	0.777
X25	0.791	X18	0.777
X7	0.788	X7	0.777
X11	0.787	X8	0.769
X20	0.787	X25	0.762

CASP3 were obtained by using the BC, CC, and DC algorithm in the cytoNCA plug-in of the software.

4.4.5. Gene Ontology (Go) Function Enrichment Analysis and the KEGG Pathway Analysis. Gene ontology function enrichment analysis was mainly based on biological processes, cellular components, and molecular function. GO enriched a total of 302 items, including 239 BP, 28 CC, and 16 MF items. Biological processes are primarily concerned with the positive regulation of the apoptotic process, negative regulation apoptotic process, positive regulation of transcription from RNA polymerase II promoterRNA, response to xenobiotic stimulus, and negative regulation of gene expression. The cellular components are mainly involved in the nucleus, cytosol, cytoplasm, plasma membrane, extracellular space, extracellular region. The molecular functions are mainly related to protein binding, identical protein binding, enzyme binding, protein homodimerization activity, DNA binding, and ATP binding (Figure 8).

A total of 78 pathways were analyzed by KEGG enrichment analysis, and the top 20 of the Count values were selected for the bubble map (Figure 9). If the bubble is red, the smaller the *P* value, and the larger the bubble, the more the number of genes. The main enriched pathways were pathways in cancer, AGE-RAGE signaling pathway in diabetic complications, MAPK signaling pathway, IL-17 signaling pathway, proteoglycans in cancer, pathways of neurodegeneration-multiple diseases, and TNF signaling pathway.

4.4.6. Molecular Docking. Active components such as procyanidin A2, procyanidin B1, and epicatechin and key targets IL6, PTGS2, TNF, EGRF, and CASP3 were screened by network pharmacology for molecular docking. The molecular docking results were evaluated by binding energy. The binding energy indicates the binding affinity between the target and the component. Binding energies <0 kcal/mol are generally considered to bind spontaneously, and smaller values of binding energy indicate a more stable binding conformation and a greater potential for interaction between the target and the component.[19,20] The three components can freely bind to the five targets (Figures 10 and 11).

5. DISCUSSION

5.1. Fingerprints. The extraction was carried out at 50 °C. The chromatographic conditions were investigated for 0.05% phosphoric acid, 0.2% phosphoric acid, 0.2% phosphoric acid, and 0.1% formic acid in methanol−water, acetonitrile−water, and aqueous phases. The chromatographic conditions of 0.05% phosphoric acid, 0.1% phosphoric acid, 0.2% phosphoric acid, and 0.1% formic acid in methanol−water, acetonitrile−water, and aqueous phase were investigated, and the mobile phase was finally determined to be acetonitrile−0.1% phosphoric

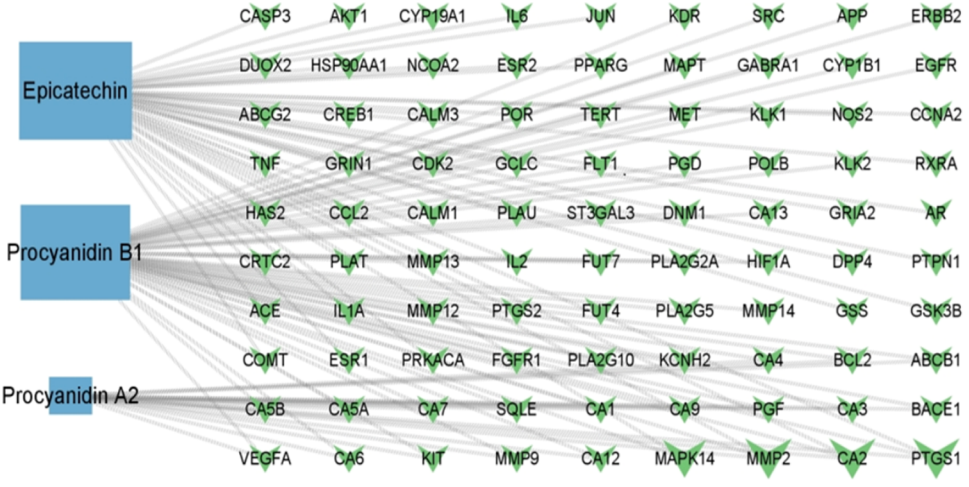

Figure 6. Composition-target network diagram.

https://doi.org/10.1021/acsomega.4c04212
ACS Omega 2024, 9, 42199−42211

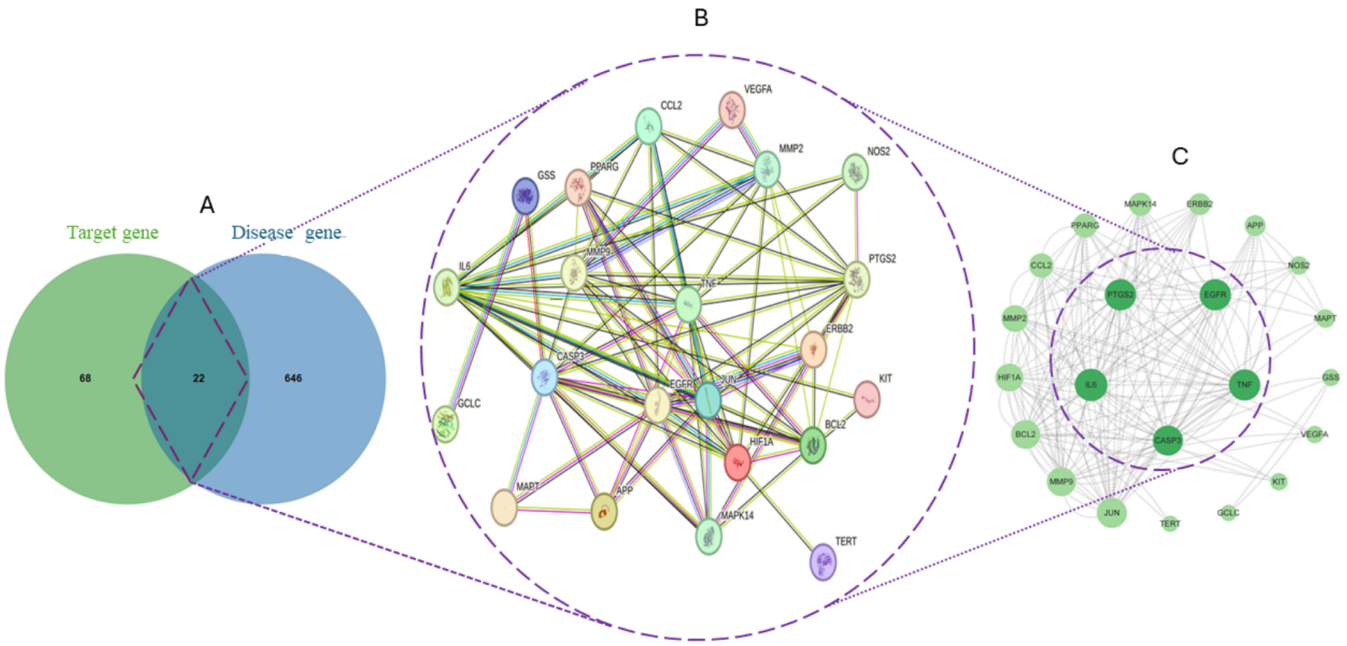

Figure 7. Collection of core targets. (A) Common target Venny diagram. (B) ppi network interaction ppi network interoperability diagram. (C) Core target map.

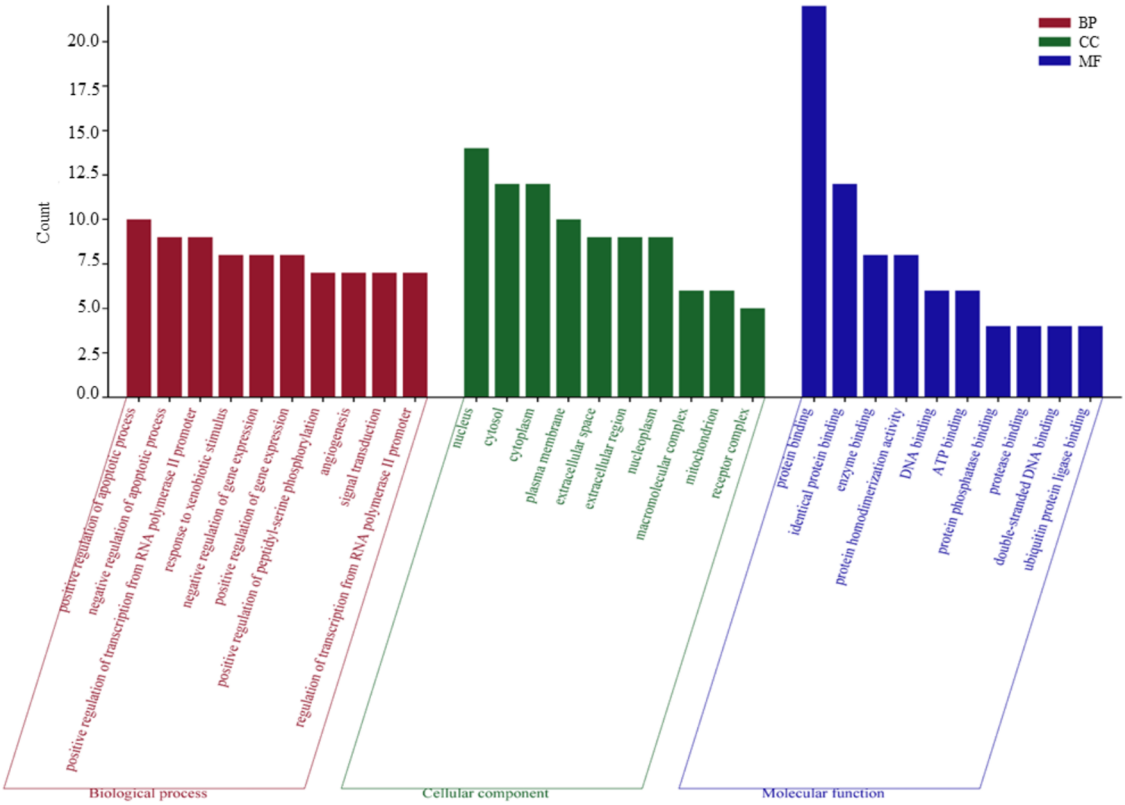

Figure 8. GO enrichment analysis.

acid−water; the detection wavelengths of the same sample were investigated, and three wavelengths of 202, 220, and 254 nm were selected. It was found that the proanthocyanidin peaks were larger and more strongly absorbed in the wavelength of 202 nm. It was found that the proanthocyanidin peak was larger at 202 nm with stronger absorption, and the detection wavelength was finally determined to be 202 nm. In this study, methanol was selected as the extraction solvent. To maximize chromatographic peak information, extraction efficiency, and method stability, we examined various extraction parameters, including the extraction method, solvent concentration, extraction time, and extraction temperature. The optimal conditions were determined to be ultrasonication using 60% methanol for an extraction time of 30 min. The 25

https://doi.org/10.1021/acsomega.4c04212
ACS Omega 2024, 9, 42199−42211

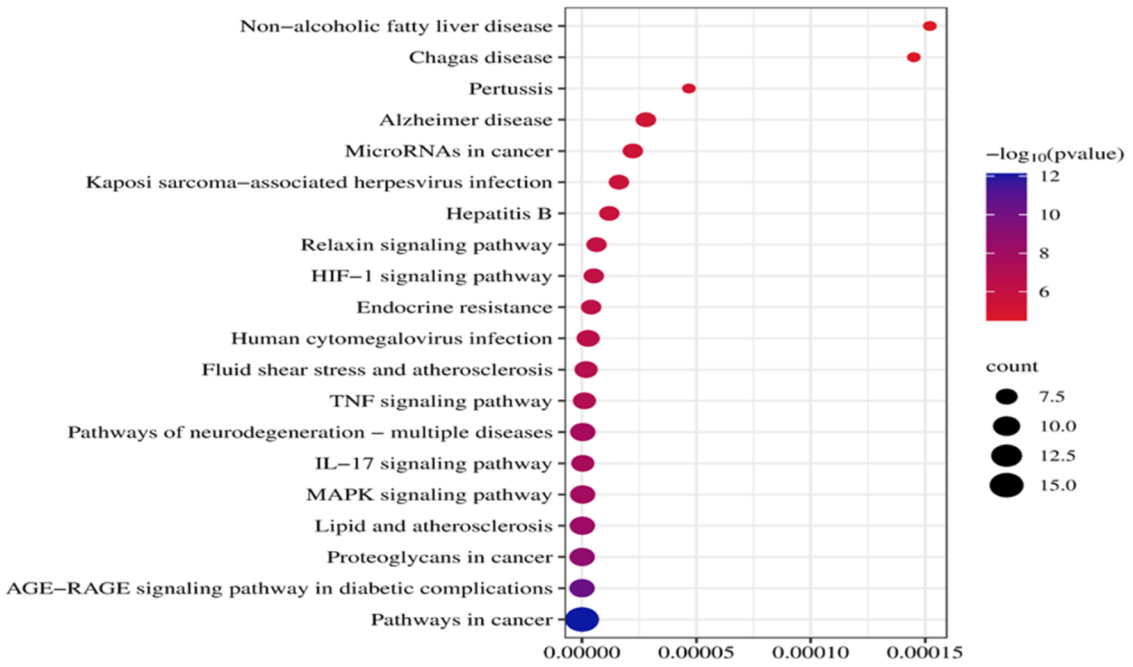

Figure 9. KEGG enrichment analysis.

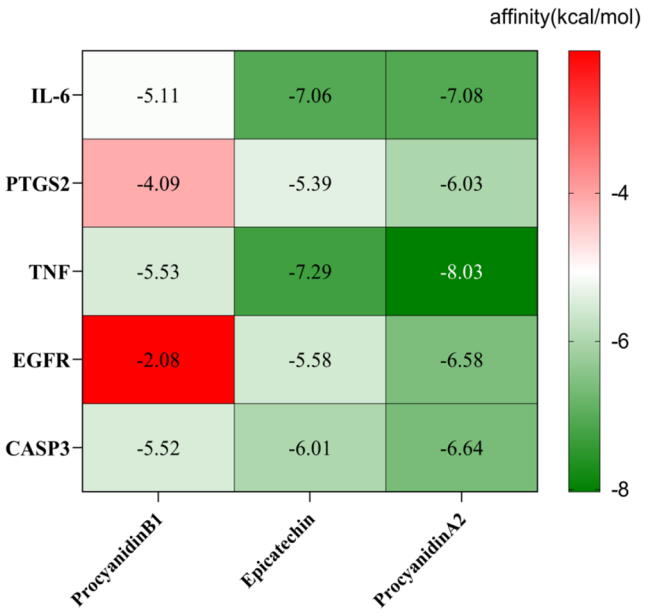

Figure 10. Binding energy of components to target molecules.

batches of samples were analyzed, 32 common peaks were determined, and 8 chemical components were identified by the standard. The similarity of the samples was between 0.920 and 0.995, indicating that the chemical components of the 25 batches of samples were stable.

5.2. Oxidation Activity. The antioxidant activity is closely related to the test system. The evaluation results of different evaluation systems have a certain degree of difference. DPPH free radical and ABTS free radical are often used as indicators to test the antioxidant activity in vitro.[21] In this study, the antioxidant activity of *IS*.Lindl was evaluated by IC_{50} of scavenging free radicals. The smaller the IC_{50}, the stronger the antioxidant activity. The scavenging effect of 25 batches of *IS*.Lindl on DPPH free radical and ABTS free radical was better, and the scavenging rate was positively correlated with the concentration.The DPPH method had stronger free radical scavenging ability than the ABTS method. In the DPPH method, compared with the positive drug (Vit C), except for S14 and S21, the IC_{50} of *IS*.Lindl from other producing areas was smaller. However, it is interesting that in the ABTS method, except for S1 and S9, the IC_{50} values of other producing areas was larger. The main reason for this phenomenon may be that the chemical composition of IS.Lind is different from the reaction mechanism of the two reagents. There are differences in the antioxidant activities of *IS*.Lindl from different habitats, indicating that the quality of medicinal materials may be affected by the climate and precipitation of different habitats.

5.3. Spectrum-Effect Relationship. Based on fingerprint and pharmacodynamics, the relationship between the components of *IS*.Lindl and antioxidant activity was established by the PLSR method and GRA. The results showed that X2, X4 (proanthocyanidin B1), X11 (epicatechin), X14, X19, X20, X23, X24, X25, X26 (proanthocyanidin A2), and X32 were positively correlated with DPPH free radical scavenging ability. Interestingly, X1, X5 (proanthocyanidin B3), X6, X7 (catechin), X9 (proanthocyanidin B4), X11 (epicatechin), X12, X15, X20, X21, X24, and X26 (proanthocyanidin A2) were positively correlated with ABTS free radical scavenging, indicating that the higher the content of the above characteristic peaks, the stronger the antioxidant capacity. It also shows that the antioxidant activity of *IS*.Lindl is the result of multicomponent synergy. Unfortunately, this study has some limitations. In this study, only some chromatographic peaks were identified. The next step will continue to use high-performance liquid chromatography−mass spectrometry (HPLC-MS) to qualitatively and quantitatively analyze the chromatographic peaks with large antioxidant contribution.

5.4. Network Pharmacology. For predicting the potential targets and pathways for the treatment of diseases by the ingredients contained in Chinese herbal medicines and constructing the links between compounds, targets, diseases,

https://doi.org/10.1021/acsomega.4c04212
ACS Omega 2024, 9, 42199−42211

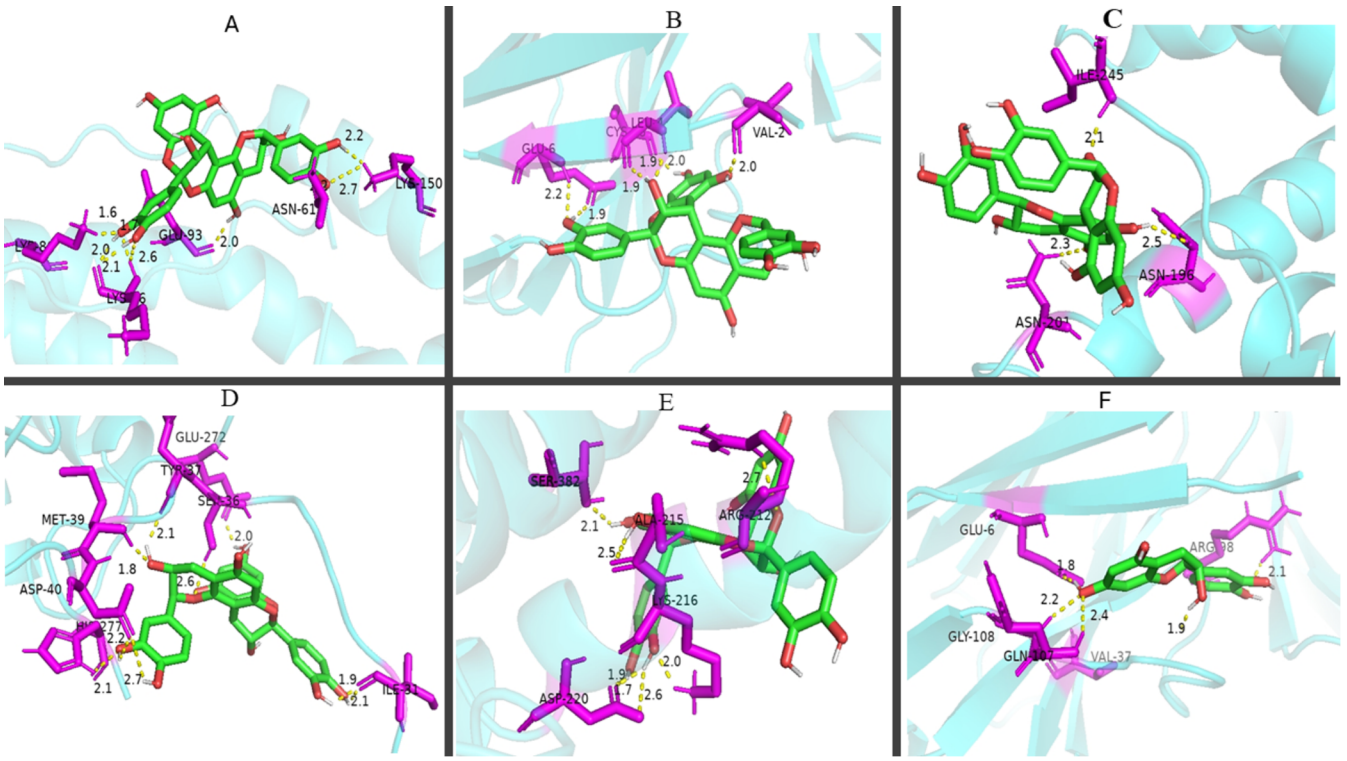

Figure 11. Partial molecular docking diagram. (A) Procyanidin A2−EGFR binding affinity; (B) procyanidin A2−IL6 binding affinity; (C) procyanidin A2−PTGS2 binding affinity; (D) procyanidin A2−TNF binding affinity; (E) procyanidin A2−CASP3 binding affinity; and (F) epicatechin−TNF binding affinity.

and signaling pathways, targeted pharmacological research is carried out. The presence of a large number of phenyl hydroxyl structures in proanthocyanidin molecules has a strong antioxidant and free radical scavenging ability, and proanthocyanidins inhibit oxidative stress damage and redox chain reactions by scavenging oxidized substances such as ROS.[22,23] Network pharmacology studies indicate that the core targets are mainly IL6, PTGS2, TNF, EGFR, and CASP3. Studies have shown that large amounts of ROS are generated during the inflammatory response, causing oxidative stress in the body, and that IL6 and TNF are proinflammatory factors that direct inflammation. These proinflammatory factors may play a role in promoting oxidative damage in the body.[24] PTGS2, also known as prostaglandin H2, is an important regulator of oxidative stress response and plays an important role in oxidative stress injury.[25,26] Oxidative stress is closely related to apoptosis. CASP3, a pro-apoptotic protein, plays a key role in this process. When a cell is damaged, its mitochondrial membrane becomes disrupted, leading to the release of cytochrome c into the cytoplasm. This release activates CASP3, which then induces apoptosis.[27,28] KEGG enrichment analysis reveals that pathways in cancer, IL-17 signaling pathway, TNF signaling pathway, MAPK signaling pathway, relaxin signaling pathway, and P13K/Akt are associated with antioxidants. Among them, IL-17 and TNF are mainly involved in the inflammatory response, and inflammation is closely related to oxidative stress. PI3K-Akt signaling pathway is one of the important pathways in the body to resist antioxidative stress and acts on Nrf2-associated antioxidant signaling to avoid cellular damage by oxidative stress.[29] The molecular docking results showed that procyanidin B1 and epicatechin procyanidin A2 had stronger affinity with the key targets of IL6, TNF, and CASP3, and the binding energies were all less than −5.0 kcal/mol, with better docking activities, which further verified that *IS*.Lindl exerted its antioxidant effects through multicomponents, multitargets, and multipathways.

6. CONCLUSIONS

Based on the results of a comprehensive analysis of spectrum-effect relationship, the partial least-squares regression coefficient was positive, and the gray correlation degree was greater than 0.8 as the standard. The antioxidant components of *IS*.Lindl were mainly proanthocyanidin B1, epicatechin, and proanthocyanidin A2. It shows that the substances that exert antioxidant activity may be the above components, revealing the material basis for the antioxidant activity of *IS*.Lindl. These components play a role by regulating IL6, PTGS2, TNF, and other targets through pathways in cancer, HIF-1 signaling pathway, MAPK signaling pathway, PI3K-Akt signaling pathway, and other signaling pathways.

AUTHOR INFORMATION

Corresponding Authors

Guo Feng − *Guizhou University of Traditional Chinese Medicine, Guiyang 550025 Guizhou, China*; Email: 453989352@qq.com

Yuchen Liu − *Guizhou University of Traditional Chinese Medicine, Guiyang 550025 Guizhou, China*; orcid.org/0000-0003-0125-5067; Email: lyc8564732@163.com

Authors

Gang Liu − *Guizhou University of Traditional Chinese Medicine, Guiyang 550025 Guizhou, China*

Lingli Zhou − *Guizhou University of Traditional Chinese Medicine, Guiyang 550025 Guizhou, China*

https://doi.org/10.1021/acsomega.4c04212
ACS Omega 2024, 9, 42199−42211

Kailang Mu − *Guizhou University of Traditional Chinese Medicine, Guiyang 550025 Guizhou, China*
Leqiang Peng − *Guizhou University of Traditional Chinese Medicine, Guiyang 550025 Guizhou, China*
Fei Ran − *Guizhou University of Traditional Chinese Medicine, Guiyang 550025 Guizhou, China*

Complete contact information is available at: https://pubs.acs.org/10.1021/acsomega.4c04212

Author Contributions

†Corresfirst author.

Notes

The authors declare no competing financial interest.

■ ACKNOWLEDGMENTS

This article is supported by the National Natural Science Foundation of China (U1812403).

■ ABBREVIATIONS

IS.Lindl, *Indigofera stachyoides* Lindl; UPLC, ultraperformance liquid chromatography; TCM, traditional Chinese medicine; DPPH, 1,1-diphenyl-2-trinitrophenylhydrazine; ABTS, 2,2-biazobis(3-ethyl-phenylpropylthiazole-6-sulfonate); PLSR, partial least-squares regression analysis; GRA, gray correlation analysis; IC_{50}, half maximal inhibitory concentration; VIP, variable importance in projection; TCMSP, traditional Chinese medicine systems pharmacology; ITCM, integrated traditional Chinese medicine; OMIM, online mendelian inheritance in man; PPI, protein−protein interaction network; BC, betweenness centrality; CC, closeness centrality; DC, degree centrality; GO, gene ontology; BP, biological process; CC, cellular component; MF, molecular function; KEGG, Kyoto Encyclopedia of Genes and Genomes; EGFR, epidermal growth factor receptor; CASP3, caspase-3; IL6, interleukin 6; PTGS2, prostaglandin-endoperoxide synthase 2; TNF, tumor necrosis factor; ROS, reactive oxygen species

■ REFERENCES

(1) Liao, Z. Y.; Fu, J.; Fu, X. H.; et al. Research Progress On Chemical Constitsuents and Pharmacological Effects of Indigofera stachyolides Lindl.and Predictive Analysis of Q-marker. *Chin. Journalpharm Ethnomed. Ethnopharm.* **2023**, *32* (12), 37−47.
(2) Zhang, Y. F.; Zav, N. L.; Zhu, Z. X.; et al. Flavonoids from roots of Miao medicine Indigofera stachyodes. *Chin. Herb. Med.* **2021**, *52* (12), 3485−3492.
(3) Li, K. M.; Liu, Y. C.; Liu, G.et al.Research Progress of Miao Medicine Indigera Stachyodes and Prediction Analysis of Q-Marker *Asia Pacific Traditional Med.* 2023; Vol. *19* 05, pp 68−75.
(4) Dan, C. L.; Zhang, Y. Y.; Zhang, Y. P.et al.Study On anti-inflammatory activity of Radix Indigofera extract based on transgenic zebrafish mode-screening *LIshizhen Med. Res.* 2016; Vol. *27* 11, pp 2617−2620.
(5) Yang, H.; Yang, Y. S.; Pang, F.et al.Effects of ethyl acetate extracts from Indigofera stachyoides Radix against carbon teteachloride induced liver injury in mice *LIshizhen Med. Res.* 2018; Vol. *29* 10, pp 2354−2357.
(6) Fu, J.; Fu, H. X.; Zhang, Y. P.et al.Extraction,separation and antibacterial activity analysis of total flavonoids from Miao medicine Indigofera stachyoides *Guizhou Sci.* 2020; Vol. *38* 06, pp 4−8.
(7) He, J. Y.; Chen, X.; Yang, L.et al.Effect of Indigofera staclrvoides extract and its preparation ov antioxidant capacity in aging mice model induced by galactose combined with sodium nitrite *Guizhou Sci.* 2022; Vol. *40* 03, pp 37−42.
(8) Zhu, W. Q.; Yin, X.; Wang, Z. H.et al.Chemical constituents and antioxidant activity coicis semen *Chin. Pharm. J.* 2023; Vol. *58* 22, pp 2054−2061.
(9) Ji, H.; Chen, M. W. Relevant Research of Reactive Oxygen species and tumor stem cell. *Chin. J. Clin.* **2017**, *11* (23), 2462−2465.
(10) Zhang, Z. J.; Wang, F. H.; Zeng, X. X. In vitro antioxidant activities and Hepatoprotective effects of Polysacchardes from allium macrostemon bunge. *Modery Food Sci. Technol.* **2014**, *30* (1), 1−6.
(11) Li, S.; Huang, X.; Li, Y.; et al. Spectrum-Effect Relationship in Chinese Herbal Medicine: Current Status and Future Perspectives. *Crit. Rev. Anal. Chem.* **2023**, *21*, 1−22.
(12) Mu, K.-l.; Li, L.; Chen, Y.; et al. Analysis of Chemical Constituents of Miao Ethnomedicine Heiguteng Zhuifeng Huoluo Capsule (HZFC) and the Discovery of Active Substances in the Treatment of Rheumatoid Arthritis. *ACS Omega* **2024**, *9* (9), 10860−10874.
(13) Khanna, S.; Selvaraj, D.; Tyagi, M.; et al. An integrated network pharmacology and molecular modelling study of phytoconstituents targeting Alzheimer's disease. *Med. Omics* **2024**, 100031.
(14) Liu, X.; Wang, Y.; Ge, W.; et al. Spectrum−effect relationship between ultra-high-performance liquid chromatography fingerprints and antioxidant activities of Lophatherum gracile Brongn. *Food Sci. Nutr.* **2022**, *10* (5), 1592−1601.
(15) He, J.; Shang, F. H.; Li, L. Y.et al.Establishment of fingerprints and spectrum-effect relationship of antioxidant activity of citri sarcodactylis fructus *Chin. Herbal Med.* 2023; Vol. *54* 23, pp 7841−7852.
(16) Liu, W.; Qin, J. P.; Pan, Z. Z.et al.Spectrum-activity relationships of anti-inflammatory effect in vitro for extracts of ampelopsis grossedentata based upon grey relational analysis *Chin. J. Hospital Pharm.* 2021; Vol. *41* 20, pp 2071−2075.
(17) Wu, M. Y.; Chen, H. F.; Cheng, R. R.; et al. Screening antioxidative material basis of total flavonoids from stems and leaves of chrysanthemum morifolium based on the spectrum-effect relationship and its mechanism. *Nat. Prod. Res. Dev.* **2024**, *36* (3), 464−477.
(18) Kang, D. D.; Zhang, R. R.; Zhan, H. P.et al.Investgation of active ingredients of Lamiophlomis Roatta(Benth.)Kudo Against Ear swelling Based on spectrum-effect relationship *Pharmacol. Clin. Chin. Mater. Med.* 2024; Vol. *40* 03, pp 1−17.
(19) Zhang, W.; Sun, M.; Lv, G.; et al. Exploring the mechanism of tenghuang jiangu wan in osteoporosis treatment based on network pharmacology, molecular docking and experimental pharmacology. *Chin. J. Anal. Chem.* **2024**, *52* (1), 100351 DOI: 10.1016/j.cjac.2023.100351.
(20) Zhou, Y. J.; Liao, S. S.; Gao, P.; et al. Mechanism of curcumae Rhizoma-Trionycis Carapax drug pair in the treatment of liver fibrosis based on network pharmacology,molecular docking and experiment validation. *Nat. Prod. Res. Dev.* **2024**, *36* (5), 856−867.
(21) Wang, J. M. Spectrum-effect relation of antioxidant activity of Flos Carthami based on DPPH, ABTS and FRAP assay. *Chin Pharm. J.* **2017**, *52* (10), 825−831.
(22) Xia, N.; Xie, C. Y.; Huang, W.; et al. Procyanidins in Peanut Red Coat: Optimization of extraction process by response surface methodology and antioxidant activity. *Food Res. Dev.* **2023**, *44* (20), 98−106.
(23) Chen, J. *Neuroprotective Mechanism of Procyanidins Mediated by Nrf2/ARE Signaling Pathway on PC12 Cells and Zebrafish Model*; Zhejiang University, 2023.
(24) Xia, S. J.; Sun, T.; Wu, J. Z.Free radical, inflammation and aging *Practical Geriatrics* 2014; Vol. *28* 02, pp 100−103.
(25) Jia, X.; Shao, W.; Tian, S. Berberine alleviates myocardial ischemia−reperfusion injury by inhibiting inflammatory response and oxidative stress: the key function of miR-26b-5p-mediated PTGS2/MAPK signal transduction. *Pharm. Biol.* **2022**, *60* (1), 652−663.
(26) Chu, J.; Liu, C. X.; Song, R.; Li, Q. L. Ferrostatin-1 protects HT-22 cells from oxidative toxicity. *Neural Regener. Res.* **2020**, *15* (3), 528−536, DOI: 10.4103/1673-5374.266060.

(27) Lakhani, S. A.; Masud, A.; Kuida, K.; et al. Caspases 3 and 7: Key Mediators of Mitochondrial Events of Apoptosis. *Science* **2006**, *311* (5762), 847−851.
(28) Cho, S. O.; Lim, J. W.; Kim, H. Oxidative stress induces apoptosis via calpain- and caspase-3-mediated cleavage of ATM in pancreatic acinar cells. *Free Radical Res.* **2020**, *54* (11−12), 799−809.
(29) Shiau, J. P.; Chuang, Y. T.; Cheng, Y. B.; et al. Impacts of Oxidative Stress and PI3K/AKT/mTOR on Metabolism and the Future Direction of Investigating Fucoidan-Modulated Metabolism. *Antioxidants* **2022**, *11* (5), 911 DOI: 10.3390/antiox11050911.

https://doi.org/10.1021/acsomega.4c04212
ACS Omega 2024, 9, 42199−42211